Journal Pre-proofs

Artificial neural network based fatigue life assessment of friction stir welding AA2024-T351 aluminum alloy and multi-objective optimization of welding parameters

Reza Masoudi Nejad, Nima Sina, Danial Ghahremani Moghadam, Ricardo Branco, Wojciech Macek, Filippo Berto

Please cite this article as: Masoudi Nejad, R., Sina, N., Ghahremani Moghadam, D., Branco, R., Macek, W., Berto, F., Artificial neural network based fatigue life assessment of friction stir welding AA2024-T351 aluminum alloy and multi-objective optimization of welding parameters, *International Journal of Fatigue* (2022), doi: https://doi.org/10.1016/j.ijfatigue.2022.106840

This is a PDF file of an article that has undergone enhancements after acceptance, such as the addition of a cover page and metadata, and formatting for readability, but it is not yet the definitive version of record. This version will undergo additional copyediting, typesetting and review before it is published in its final form, but we are providing this version to give early visibility of the article. Please note that, during the production process, errors may be discovered which could affect the content, and all legal disclaimers that apply to the journal pertain.

Artificial neural network based fatigue life assessment of friction stir welding AA2024-T351 aluminum alloy and multi-objective optimization of welding parameters

Reza Masoudi Nejad[1,*], Nima Sina[2], Danial Ghahremani Moghadam[3,*], Ricardo Branco[4], Wojciech Macek[5], Filippo Berto[6]

[1]School of Mechanical and Electrical Engineering, University of Electronic Science and Technology of China, Chengdu, 611731, China

[2]Department of Mechanical Engineering, Najafabad Branch, Islamic Azad University, Isfahan, Iran

[3]Faculty of Engineering, Department of Mechanical Engineering, Quchan University of Technology, Quchan, Iran

[4]University of Coimbra, CEMMPRE, Department of Mechanical Engineering, Coimbra, Portugal

[5]Gdansk University of Technology, Faculty of Mechanical Engineering and Ship Technology, 11/12 Gabriela Narutowicza, Gda´nsk 80-233, Poland

[6]Department of Mechanical and Industrial Engineering, NTNU – Norwegian University of Science and Technology, Trondheim, Norway

Abstract

In this paper, the fracture behavior and fatigue crack growth rate of the 2024-T351 aluminum alloy has been investigated. At first, the 2024-T351 aluminum alloys have been welded using friction stir welding procedure and the fracture toughness and fatigue crack growth rate of the CT specimens have been studied experimentally based on ASTM standards. After that, in order to predict fatigue crack growth rate and fracture toughness, artificial neural network is used. To obtain the best neuron number in the hidden layer of the artificial neural network, different neuron numbers are tested and the best network based on the performance is selected. Then the fitting method is applied and the fitted surfaces that illustrate the behavior of welding are shown and the results of artificial neural network and fitting method are compared. Also, multi-objective optimization algorithm is used to obtain the best welding parameters and finally sensitivity analysis is applied to measure the effect of rotational and traverse speeds on the fracture toughness and fatigue crack growth rate.

Keywords: Friction stir welding; Artificial neural network; Fatigue life; Aluminum alloy; Fracture toughness.

1. Introduction

The fatigue life of engineering components is determined by the sum of the cycles required to initiate the fatigue crack and its growth from the initial length to the critical length. The final

---

*Corresponding authors.

E-mail addresses: masoudinejad@uestc.edu.cn (R. Masoudi Nejad), d.ghahremani@qiet.ac.ir (D. Ghahremani Moghadam), ricardo.branco@dem.uc.pt (R. Branco), wojciech.macek@pg.edu.pl (W. Macek), filippo.berto@ntnu.no (F. Berto).

stage of failure provides the final conditions in the engineering component [1-4]. High strength-to-weight ratio make aluminum one of the suitable materials for engineering applications; But one of the problems with the use of aluminum is the inadequacy of traditional methods for welding this metal. Friction stir welding (FSW) is a solid-state joining process that was invented and is currently used as one of the most widely used aluminum alloy welding processes. FSW is a high-speed joining process and has the ability to be mechanized, which will save cost and time. Due to the increasing use of FSW method in different industries [5] it is necessary to investigate the fracture and fatigue properties of friction stir welded joints using appropriate experimental and numerical methods. Many studies have investigated the effect of welding parameters on the mechanical properties of FSW joints. The researches investigate that for each range of traverse speeds, there is a particular range of rotation speed that generates welds with the least number of defects and superior mechanical properties [6]. By investigating the correlation of welding parameters and joints properties, suitable welding conditions can be designated [7]. Rajakumar et.al [8] for different aluminum alloys proposed an empirical relationship to predict the optimized FSW process parameters and defect free joints. Radisavljevic et.al [9] studied the tensile efficiency of the FSW joints obtained is in the range of Rotational (R) and traverse speeds (v). The results revealed that the best welds quality is obtained at the specified ratio of R/v. Dong et al. [10] showed that increasing the welding traverse speed increases the tensile strength of 6005 aluminum alloy specimens. This conclusion can be justified due to the increase of some hardening sediments. Based on the results of Kundu et al. [11] high tool rotational speed caused to smooth welding as compared to lower rotational speed of the tool. Moshwan et al. [12] concluded that increasing the rotational speed of FSW reduces the tensile properties of welds. Higher solubility of β-Mg_2-Al_3 hardening sediments at higher rotational speeds (higher heat input) reduces the welds strength.

Fracture mechanics is widely used to predict the FCG [13-18] and several researchers have improved models to predict the stress intensity factors (SIFs) and fatigue life [19-22]. Considering the advantages of FSW compared to traditional welding methods and also the superior mechanical properties, it has been shown that the fracture toughness of friction stir welded joints is higher than traditional methods such as TIG and MIG [23]. Kulekci et al. [24] investigated the fracture toughness of friction stir welded lap joints of 6063 and 2014 alloys. Their results show that the fracture toughness of lap joints decreases exponentially with hardness increasing. One of the main factors that influencing the fatigue crack growth rate in friction stir welds is welding residual stresses [25] and what affects the values of welding

residual stresses is FSW process parameters. Fatigue crack growth develops due to repeated loads or a combination of loads and environmental factors. This causes the crack growth rate to increase with time [26-29]. D'Urso et al. [30] results showed that non-optimal FSW parameters caused to higher fatigue crack growth rate at middle and high values of stress intensity factor, due to some defects, such as tunnels and keyholes. Also, some researches investigate the effects of FSW process defects that affect the fatigue performance [31, 32]. Kim et al. [33] by investigating the effects of FSW parameters, found that fatigue resistance decreases with increasing tool traverse and rotational speed. The results of Cirello et al. [34] showed that the ratio of traverse speed to rotational speed (R/v) in FSW is the most effective parameter in affecting of the mechanical properties and fatigue performance of the FSW joints. Hrishikesh et al. [35] investigated the high cycle fatigue behavior in FSW joints of 6061 aluminum alloy and found that the bond strength in the fatigue loading is approximately 40% of the static loading mode; Also, increasing the welding rotational speed reduces the fatigue life. Okuyucu et al. [36] developed an Artificial Neural Network (ANN) model for prediction of mechanical properties of FSWed joints in terms of welding speeds. Ghasemi et al. [37] considering the number of passes, rotational speed, traverse speed, and addition of nano-sized Al_2O_3 powder in FSW of the mild steel as the input parameters could predict the microhardness of the stir zone of the welds as the output parameter using an ANN model. Dinaharan et al. [38] described the wear rate of the friction stir processed of AA6082 AMCs reinforced specimens in terms of process parameters (welding speed, groove width, type of ceramic particle) via an ANN model. Hartl et al. [39] investigated the possibilities and limits of prediction the surface quality of FSW of the aluminum alloy EN AW-6082 T6 joints using an ANN model. Dehabadi et al. [40] studied the effects of FSW tool's profile on the microhardness of the AA6061 welds employing ANN technique. Some researchers investigated the correlation between tensile strength of the FSW joints as the outputs and the process parameters such as welding speed and tool properties as the inputs, utilizing ANN models [41-45]. Also, some researchers studied the capability of the ANN technique to predict the microstructure in the FSW joints [46-48]. However, in recent years, less research has been done on the precise optimization and prediction of the FSW process parameters in terms of fracture and fatigue properties of the joints. One of the most important parameters in the study of fracture behavior of the FSW joints is the fracture toughness and also in the study of fatigue crack growth behavior of the joints is the FCP rate. Artificial Neural Networks (ANN's) are used in different mechanical applications. These networks can predict the behavior of complex systems especially systems with non-linear behavior. Artificial Neural Networks firstly were

3

inspired by the human brain. In the late 1940s D.O.Hebb introduced the Hebbian learning rule [49]. In the next decade, the perceptron was created by Rosenblatt [50-53]. Artificial neural networks including several layers were introduced by Ivakhnenko and Lapa [54-56]. Werbos's backpropagation algorithm was created which leads to the practical training of multi-layer networks [57]. Hence, in the current work, using a feed-forward artificial neural network (ANN), the fatigue and fracture behavior of the FSW of the AA2024-T351 joints is predicted. This ANN is used to predict outputs (FCP rate and fracture toughness) based on the inputs (rotational and traverse speeds). In the next step, the ANN results are compared to the fitting method to select the better model in predicting the outputs. Then using the Non-Dominated Sorting Genetic Algorithm (NSGAII) on the model, the optimum values of rotational and traverse speeds are obtained. Finally, the sensitivity analysis is performed to evaluate the effect of each input on the outputs.

2. Materials and methods

2.1. FSW process

In this research, the alloy used for FSW is 2024-T351 aluminum alloy. Table 1 shows the chemical composition of the alloy determined using the X-ray fluorescence spectroscopy (XRF) method. The mechanical properties of the alloy are also given in Table 2. The plates used for FSW have dimensions of 120*35 mm and a thickness of 8 mm and are placed side by side along the longitudinal edge for welding.

Table 1. Percentage of 2024-T351 aluminum alloy composition determined by XRF method.

Al	Cu	Fe	Mg	Mn	Si	Zn
Base	4.45	0.29	1.53	0.72	0.11	0.12

Table 2. Mechanical properties of 2024-T351 aluminum alloy.

Tensile strength (MPa)	324
Ultimate tensile strength	429
Vickers microhardness	137
Poisson's ratio	0.31
Elasticity modulus (GPa)	77.5

The tools shown in Figure 1 were used to FSW of the plates. The tool is made of SPK2436 steel with a hardness of 50 Rockwell (HRC), the geometric characteristics of the tool are specified on the Figure 1. The tool has a tapered pin and threads with the pitch of 1 mm created on it. The tapered pin makes it easy for the tool to penetrate the workpiece and greatly reduces

the forge force required for welding, as well as the threads causes a larger volume of softened material to move with each rotation of the tool.
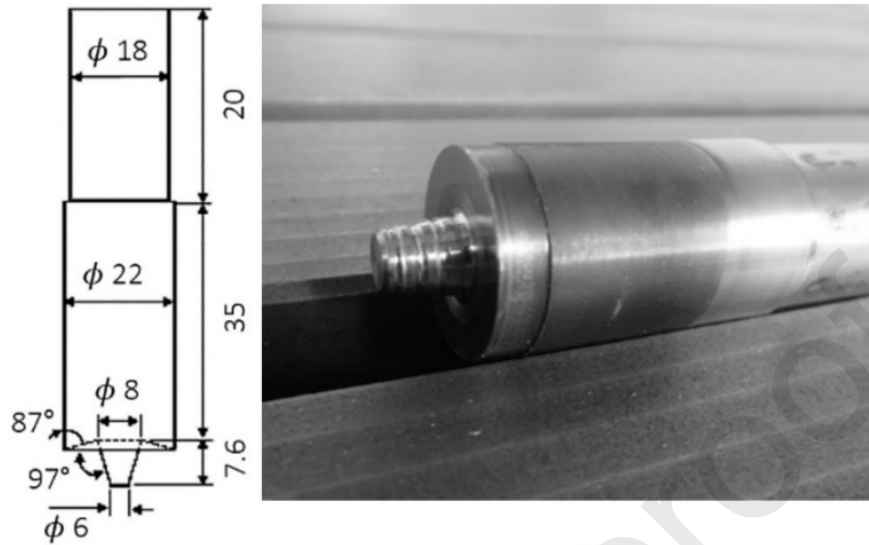

Figure 1. FSW tool and geometric characteristics of the tool (dimensions in mm).

FSW was performed with 2 tones universal MP4 milling machine. First, two aluminum plates are placed along the longitudinal edge and then fastened inside the clamps. A steel sheet is also used as the bottom support plate. The tilt angle of the tool was 2 degrees. Figure 2 shows the prepared FSW set up with a sample closed in clamps and a welded specimen after the welding.
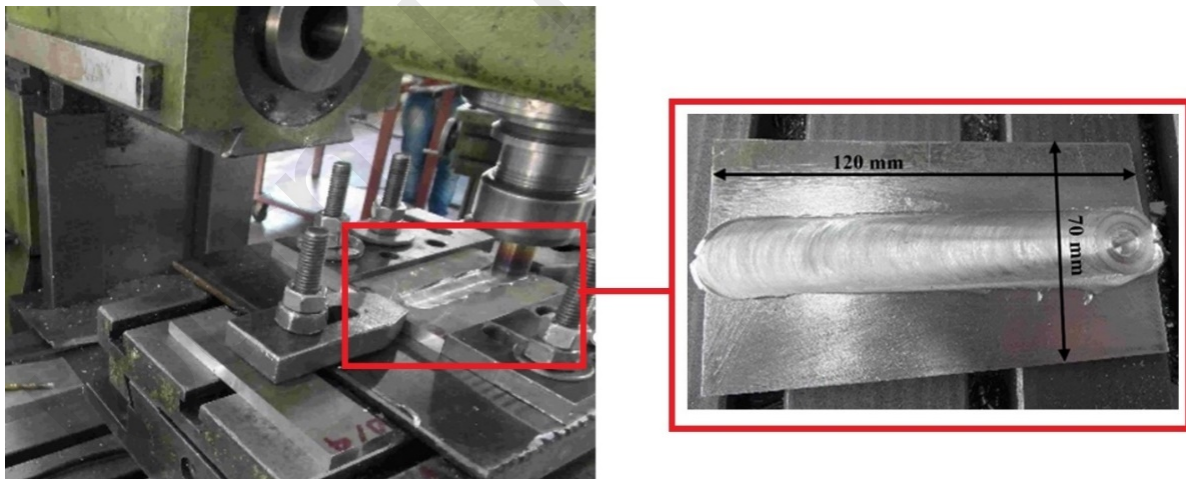

Figure 2. The prepared FSW set up and FSWed specimen.

FSW of the plates is performed with the different rotational and traverse speeds of the tool, the values of the welding speeds are given in Table 3. Rotational and traverse speeds are selected so that the final welding joints are free of any defects and cracks. Other FSW parameters are considered fix in welds.

5

Table 3. Different rotational and traverse speeds of the tool in FSW of the specimens.

Specimen no.	ω (rpm)	v (mm.min^{-1})
1	400	8
2	400	16
3	400	20
4	400	25
5	400	31.5
6	400	40
7	500	8
8	500	16
9	500	20
10	500	25
11	500	31.5
12	500	40
13	630	8
14	630	16
15	630	20
16	630	25
17	630	31.5
18	630	40
19	800	8
20	800	16
21	800	20
22	800	25
23	800	31.5
24	800	40
25	1000	8
26	1000	16
27	1000	20
28	1000	25
29	1000	31.5
30	1000	40

2.2. Fatigue crack growth test

Fatigue crack growth tests have been performed on non-welded and FSWed specimens using a universal 10-ton tensile test machine. The experiments were performed on CT specimens. To prepare the specimens, the plates were cut in the direction of rolling of the plate (L-T direction of the main plate). The plates are FSWed, then final CT specimens obtained by machining and the specimen's thickness was 6 mm. The final prepared CT specimen and the dimensions is presented in Figure 3.
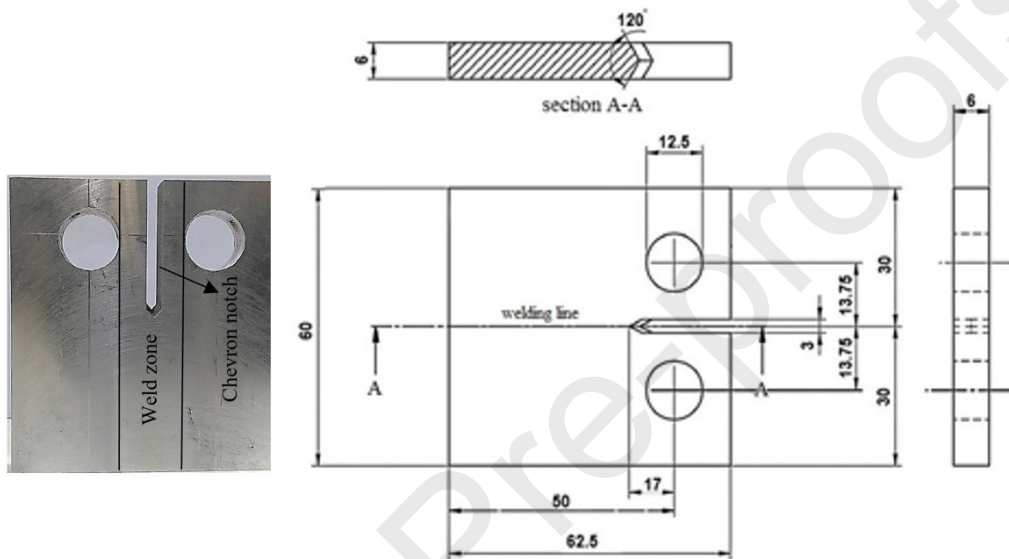

Figure 3. The final prepared CT specimen for fatigue crack growth test (dimensions in mm).

CT specimens were prepared and tested to calculate fracture toughness according to ASTM E399 [58] and to study fatigue crack growth rate according to ASTM E647 [59]. To fatigue precracking, the CT specimens were subjected to fatigue loads with a maximum of 3 kN and a minimum of 0.3 kN (R-ratio = 0.1) and a frequency of 10 Hz. The final precrack length for the fracture toughness CT specimens was 25 mm (a/w= 0.5) and for the fatigue crack growth rate CT specimens was 19 mm (a/w= 0.38). For the fracture toughness experiment, the specimens were subjected to tensile loading at a rate of 0.1 kN/sec. Figure 4 shows the load versus crack opening displacement (COD) for a number of FSW and base metal specimens. This curve is used to calculate the fracture toughness according to ASTME399.
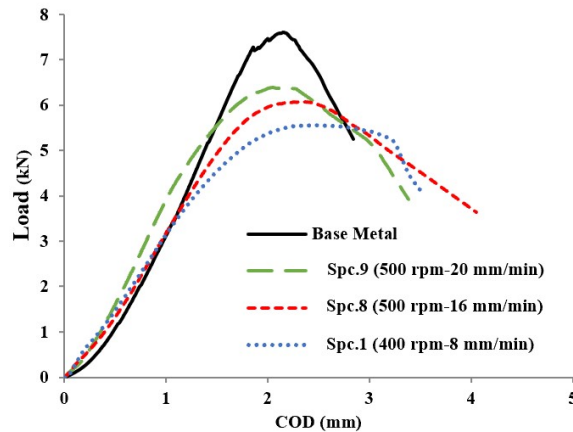
7

Figure 4. load versus crack opening displacement (COD).

FCP experiments have been performed at constant load amplitude. The maximum load is 2.2 kN and the minimum load is 0.22 kN (R-ratio = 0.1) and the loading frequency is 10 Hz. Crack length was measured using the compliance method. 31 different specimens were tested for experiments, including 30 FSW specimens with different conditions and one base metal specimen. To reduce the error, the experiments was repeated 3 times for each specimen. Totally 63 specimens were tested for fatigue crack growth rate investigation in FSW joints. The crack length versus loading cycles curve is extracted based on the incremental polynomial method. Using this curve and ASTME647, it is possible to plot fatigue crack growth rate (*da/dN*) versus stress intensity factor changes (ΔK) for the tested specimens. In this curve, using the Paris equation ($\frac{da}{dN} = c(\Delta K)^m$), the constants *c* and *m* can be calculated. The exponent *m* in Paris equation actually indicates the slope of the FCP line (in Log(*da/dN*) versus Log(ΔK) curve) and by determining this parameter in different FSW specimens, the effect of FSW parameters on the FCP rate could be investigated.

3. Artificial neural network and multi optimization of welding parameters

3.1. Artificial neural network Architecture

Neurons are the fundamental units of the nervous system which receive inputs and by a mathematical operation, the output is produced. Usually, the input is weighted and a bias is added to its value and then it passes through a non-linear function which is called the activation function. In most cases, the activation function is a sigmoid function. A mathematical model of a neuron is shown in Figure 5.
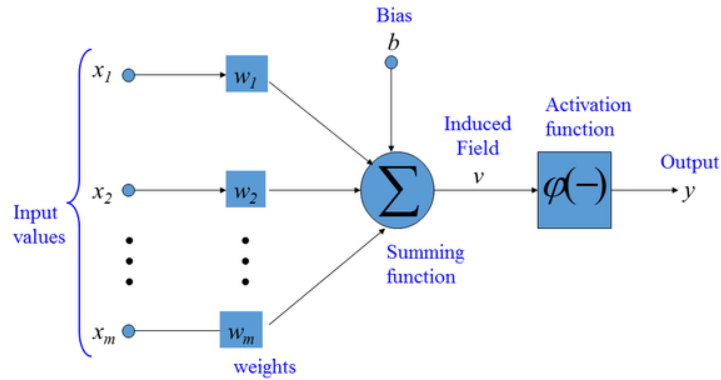
8

Figure 5. Mathematical model of artificial Neuron.

The mathematical formulation of a neuron is presented in Eq. (1).

$$y = \varphi \left(b + \sum_{i=1}^{m} x_i w_i \right) \tag{1}$$

where y is the output, φ is the activation function. x_i and w_i are the i-th input and weight respectively. Also, b is the bias. An Artificial Neuron with neurons is shown in Figure 6.
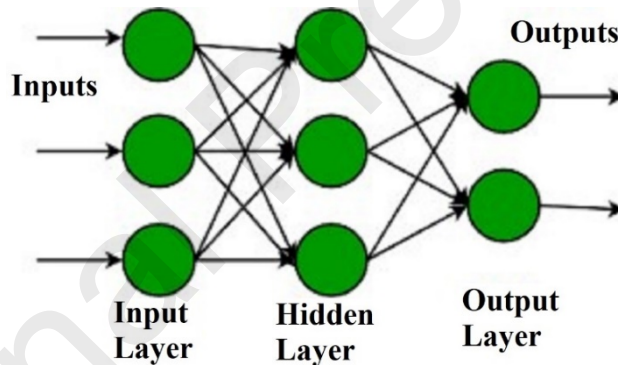

Figure 6. Artificial neural network with neurons.

It can be seen in Figure 6that the ANN consists of three layers including input, hidden and output layer. As the ANN should predict two parameters, the number of neurons in the output layer is 2. Datapoints are divided into two main categories including train and test. Train data are used to adjust the weight and biases of the ANN during the learning process. Test datapoints at the end of the learning process are introduced to the ANN for the first time. In the current work, 70 percent of data points are considered for train and the rest of data point is for the test. An accurate ANN not only should be able to predict train data points, but also it should not have any overfitting. Overfitting means that the ANN outputs of the train are close to the target values but the network fails in the test. The output of ANN depends on different parameters such as the number of neurons in the hidden layer, activation function and the learning

9

algorithm. In this paper, the activation function is considered as a tangent sigmoid function which is introduced in Eq. (2).

$$\text{tansig}(n) = \frac{2}{1 - e^{-2n}} - 1 \tag{2}$$

The learning algorithm is Levenberg-Marquardt (LMA) which is also known as the damped least-squares (DLS) method. This algorithm firstly was introduced by Kenneth Levenberg in 1944 and then rediscovered by Donald Marquardt. This algorithm is one of the most common learning algorithms in ANN's.

3.2. Optimization and NSGA-II Algorithm

Optimization is a way of finding optimum solutions of a problem. Multi-objective optimization is used when there is more than one objective function in the presence of a trade-off between two or more conflicting objects. Multi-objective optimization is formulated as:

$$\min\left(f_1(\vec{x}), f_2(\vec{x}), ..., f_k(\vec{x})\right)$$
$$s.t.\vec{x} \in X \tag{3}$$

Where k is the number of objectives and X is the decision vector. In a multi-objective problem typically, there is not a feasible solution that minimizes all objective functions. In these problems, Pareto Optimal is used which consists of solutions that cannot be improved in any of the objectives without degrading at least one of the other objectives. Although there are many classical optimization algorithms, Classical algorithms sometimes are stuck in local optimum points. In addition, the convergence of classical algorithms depends on the chosen initial point. In recent decades, powerful evolutionary optimization algorithms are introduced and improved by many researchers such as Multi-Objective Particle Swarm Optimization (MOPSO), Niched Pareto Genetic Algorithm (NPGA), Pareto Archived Evolution Strategy (PAES) and Non-Dominated Sorting Genetic Algorithm II (NSGAII) [60-63]. NSGAII as an evolutionary algorithm is a powerful algorithm and widely is used for multi-objective optimizations in engineering problems. This algorithm is inspired by the Genetic Algorithm and developed to be used for multi-objective optimization problems. NSGA-II simultaneously optimizes each objective which is not dominated by other solutions. Some researchers claimed that in this algorithm, finding the crowded distance and crowded comparison operator and non-dominated sorting are fast and simple and it can outperform many multi-objective optimizations in diversity [64]. NSGA-II is considered an evolutionary algorithm. To have a better understanding of the NSGAII algorithm some terms of this algorithm are described.

10

Mutation: Chromosomes are the proposed solutions in the problem space. Each dimension of solution in this space is called a gene. The mutation is altering one or more gene values in a chromosome from its initial state. This process increases the diversity and can help the algorithm to find new solutions.

If and only if there is no objective of P worse than that objective of Q and there is at least one objective of P better than that objective of Q. Domination in mathematic formulation is presented in Eq. (4).

$$f_i(\vec{x}_1) \le f_i(\vec{x}_2), \quad \text{for all indices}$$
$$i \in \{1, 2, ..., k\}, \quad \text{and}$$
$$f_j(\vec{x}_1) \prec f_j(\vec{x}_2), \quad \text{for at least one index}$$
$$j \in \{1, 2, ..., k\}.$$

(4)

The crowding distance of a solution is defined as the distance of each solution to its two neighboring solutions. The crowding distances in two directions are shown in Figure 7.
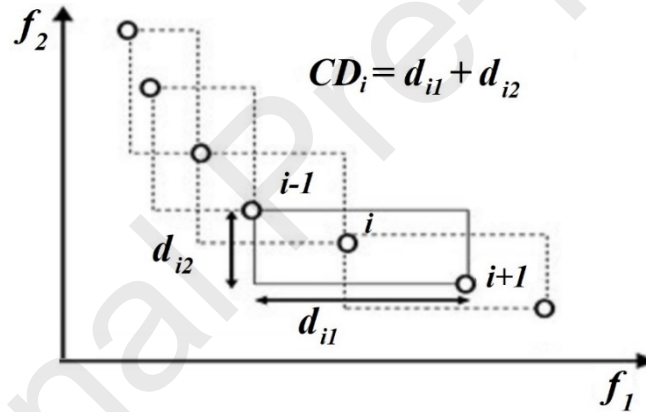

Figure 7. Crowding distance of a solution.

In multi-objective optimization problems Pareto front is a set of non-dominated solutions in the search space. Pareto is shown in the space of objective functions. The best-founded answers are in the first front are called the Pareto front. The NSGAII algorithm has some advantages such as; 1-The elites of a population have more chances to be carried to the next generation, 2- It uses crowding distance to guarantee diversity, 3- The non-dominated solutions are emphasized, and 4. Variety and efficiency are maintained.

The algorithm of NSGA_II is; 1- Initialization of Population: This is based on the constraints and the range of variables, 2- Non-dominated sorting: Sorting the population based on the domination individuals, 3- Crowding distance: After Non-dominated sorting, the crowding distances values for individuals are calculated. The individuals are selected based on the rank and crowding distance, 4-

11

Selection: The selection is based on a binary tournament or roulette wheel selection considering crowded-comparison operator, 5- Genetic Operators: Real Genetic Algorithm (GA) is used for binary crossover and mutation, and 6- Recombination and selection: Offspring population and the current generation are collected and the individuals of the next generation are defined by selection until the number of the population reaches the current population size, the new generation is filled by each front subsequently. The algorithm of NSGA_II is illustrated in Figure 8.
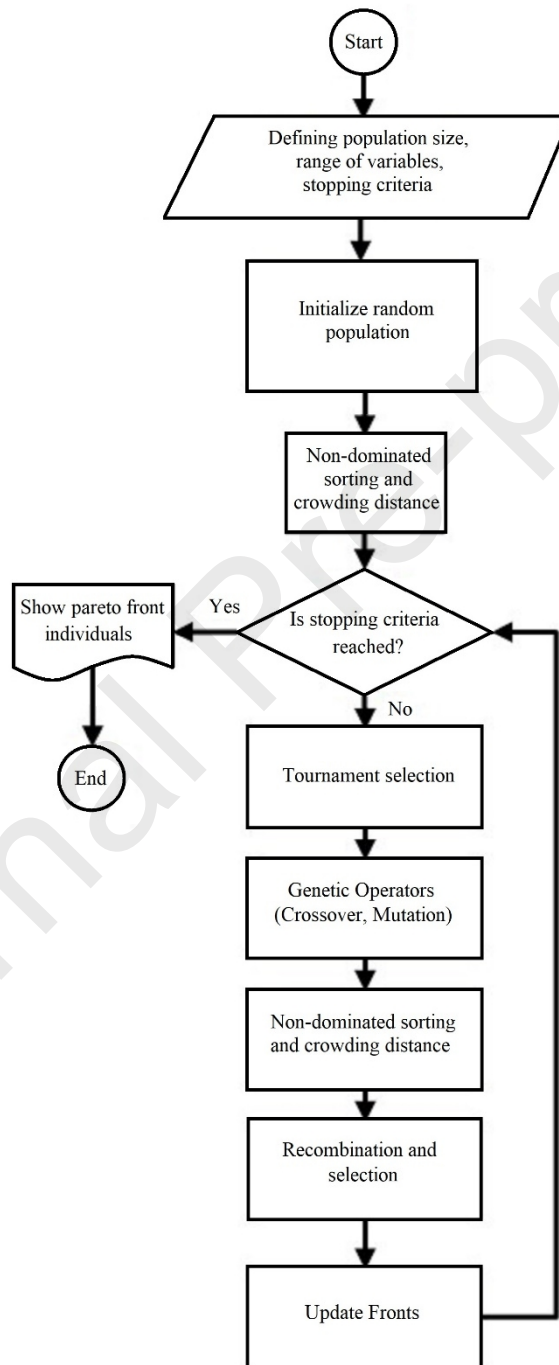

Figure 8. The algorithm of NSGA_II.

12

In this work, the cost functions are slope of FCP rate curve (*m*) and fracture toughness which can be predicted by both ANN or fitting methods. As the ANN is more accurate in prediction the behavior of this system, the ANN is used as the cost function to calculate its value based on the *ω* and *v*. The aim of this multi optimization problem is minimizing slope (*m*) and maximizing fracture toughness at the same time. The parameters of the problem space are rotational speed and traverse speed. The range of these parameters and NSGA_II settings are presented in Table 4.

Table 8. The range of parameters and algorithm settings.

Description	Maximum number of generations	Initial population size	Crossover percentage	Mutation Percentage	Mutation rate	Range of rotational speed (rpm)	Range of traverse speed (mm/min)
Value	40	100	0.7	0.4	0.02	400-1000	8-40

4. Results and discussion

4.1. Artificial neural network Results

In the current work, rotational speed and traverse speed are inputs of the ANN and the targets are fatigue crack growth rate and fracture toughness. the experimental test results are presented in Table 5. In this table, *ω* is rotational speed in rpm, *v* is traverse speed in mm/min, *m* is the slope of FCP rate curve and K_I is fracture toughness in MPa.m$^{1/2}$.

Table 5. The experimental test results.

Number	*ω* (rpm)	*v* (mm/min)	*m*	K_I
1	400	8	3.45	40.6
2	400	16	4.03	46.8
3	400	20	4.95	44.3
4	400	25	6.37	40.5
5	400	31.5	6.81	33.8
6	400	40	8.11	23.4
7	500	8	4.12	38.1
8	500	16	3.92	45
9	500	20	3.87	47.2

13

10	500	25	4.15	44.1
11	500	31.5	5.34	36.4
12	500	40	6.74	31.6
13	630	8	5.27	35.3
14	630	16	3.64	43.2
15	630	20	3.78	44.9
16	630	25	3.92	46.9
17	630	31.5	4.01	44.7
18	630	40	5.24	39.2
19	800	8	5.34	29.4
20	800	16	5.11	40.5
21	800	20	4.89	42.7
22	800	25	4.27	44.5
23	800	31.5	4.19	47.1
24	800	40	4.3	44.8
25	1000	8	7.05	22.1
26	1000	16	6.84	28.6
27	1000	20	6.32	32.7
28	1000	25	6.17	35.4
29	1000	31.5	5.82	39.7
30	1000	40	5.43	43.4

To find the best architecture of the ANN, different neuron numbers in the hidden layer are used and the output results of that neuron number are stored. As the ANN output for a specific neuron number is not always constant and in order to increase the reliability of results, for each neuron number, the ANN is run 10 times. Therefore, the performance of each neuron number is the average value of 10 times running the ANN. By running the ANN several times and calculating the performance of each run, the average performance is calculated for each neuron number and finally, the results of each neuron number based on their performances are sorted. In this ANN the performance is defined as the Mean Square Error (MSE). The error is the difference between the ANN outputs and the targets. Targets are the experimental data points. The MSE is shown in Eq. (5).

$$MSE = \frac{1}{N} \sum_{i=1}^{N} (y_i - t_i)^2 \tag{5}$$

14

where N is the number of datapoints. y_i and t_i are the ANN outputs and the targets. These sorted performances are presented in Table 6. The neuron numbers are sorted based on the performances. It can be seen that the ANN with 12 neurons in the hidden layer has the best performance.

Table 6. The performances of ANN for different neuron numbers.

Neuron Number	ANN Performance
12	0.344502614
9	1.030933701
17	1.717364787
22	2.403795874
10	3.090226961
18	3.776658047
15	4.463089134
23	5.14952022
8	5.835951307
21	6.522382394
20	7.20881348
16	7.895244567
24	8.581675654
14	9.26810674
11	9.954537827
13	10.64096891
19	11.3274

4.2. Correlation Coefficient

Another criterion to judge the accuracy of predicted values is the correlation coefficient. The correlation coefficient is a measure of linear correlation between two sets of data and its value is between -1 to 1. The correlation coefficient formula is presented in Eq. (6).

$$r = \frac{\sum_{i=1}^{n}(x_i - \bar{x})(y_i - \bar{y})}{\sqrt{\sum_{i=1}^{n}(x_i - \bar{x})^2 \sum_{i=1}^{n}(y_i - \bar{y})^2}} \tag{6}$$

15

where r is the correlation coefficient, x_i is the values of the target of a sample, $\bar{x}$ is mean values of the target, y_i is values of the output in a sample and $\bar{y}$ is the mean values of the outputs. A positive correlation coefficient indicates a positive relationship and a negative value signifies a negative relationship between two datasets. A value of zero for the correlation coefficient means that there is no relationship between the two variables. Therefore, in the best case, the correlation coefficient is 1. In Table 7 the correlation coefficient for m and K_I for train and test data points are shown. Considering Table 7, it can be seen that the correlation coefficient for m and K_I for both train and test ANN results are very close to 1 which means that the ANN results are compatible to the targets.

Table 7. The correlation coefficients.

Neuron Number	m Train	m Test	K_I Train	K_I Test
12	0.987903308	0.987503551	0.993172041	0.989401676
9	0.986344485	0.912348643	0.950936805	0.944292183
17	0.941962115	0.891673619	0.945819032	0.9220673
22	0.937404979	0.890357635	0.937959223	0.90012256
10	0.929061331	0.876078936	0.927803903	0.895258849
18	0.917563033	0.874206954	0.919020434	0.878213563
15	0.913156517	0.868324107	0.908856293	0.876816529
23	0.910171176	0.867667596	0.89096764	0.874346001
8	0.909521799	0.865366371	0.890888674	0.863221964
21	0.906832813	0.853800809	0.879059215	0.837343991
20	0.902869012	0.849040226	0.87223049	0.829936697
16	0.884858026	0.830172466	0.865154674	0.821125318
24	0.883851169	0.811679025	0.859319945	0.821027222
14	0.877348914	0.809065102	0.853724182	0.814147615
11	0.856005004	0.790645643	0.849493221	0.797559982
13	0.840624978	0.779984	0.839342434	0.789561355
19	0.835035675	0.777444903	0.827328072	0.769318818

4.3. Surface Fitting Method

Another method to predict data points is the curve fitting method. But as in this case, there are two inputs including rotational speed and traverse speed, a surface should be fitted on data points. It should be noted that as there are two outputs including slope of FCP rate curve and

16

fracture toughness, two separate surfaces are proposed for predicting the outputs. A surface for m and a surface for K_I. The equations of the fitted surfaces for m and K_I are presented in Eq. (7), respectively.

$$
\begin{aligned}
Fitted\_surface(x, y) = {} & p_{00} + p_{10}x + p_{01}y + p_{20}x^2 + p_{11}xy + p_{02}y^2 + p_{30}x^3 + p_{21}x^2y \\
& + p_{12}xy^2 + p_{03}y^3 + p_{40}x^4 + p_{31}x^3y + p_{22}x^2y^2 + p_{13}xy^3 + p_{04}y^4 \\
& + p_{41}x^4y + p_{32}x^3y^2 + p_{23}x^2y^3 + p_{14}xy^4 + p_{05}y^5
\end{aligned} \tag{7}
$$

where x represents rotational speed and y represents traverse speed. By performing surface fitting, the coefficients of Eq. (7) for m and K_I are obtained and presented in Table 8. The fitted surfaces for m and K_I are depicted in Figure 9.

Table 8. The coefficients of the fitted surfaces for m and K_I based on the Eq. (7).

| Coefficients	Fitted surface of m	Fitted surface of K_I
p_{00}	-4.927	-35.83
p_{10}	0.001843	0.442
p_{01}	1.992	7.219
p_{20}	0.0001649	-0.001
p_{11}	-0.0125	-0.03706
p_{02}	0.04094	-0.00116
p_{30}	-3.30E-07	9.18E-07
p_{21}	1.68E-05	7.12E-05
p_{12}	0.0001226	0.000662
p_{03}	-0.002017	-0.01249
p_{40}	1.70E-10	-3.03E-10
p_{31}	7.23E-10	-5.82E-08
p_{22}	-5.96E-07	-7.36E-07
p_{13}	8.45E-06	-1.77E-06
p_{04}	-3.21E-05	0.00032
p_{41}	-5.57E-12	1.64E-11
p_{32}	2.97E-10	2.45E-10
p_{23}	-1.05E-09	4.72E-09
p_{14}	-6.80E-08	-8.41E-08
p_{05}	7.08E-07	2.18E-06

17

(a)

(b)
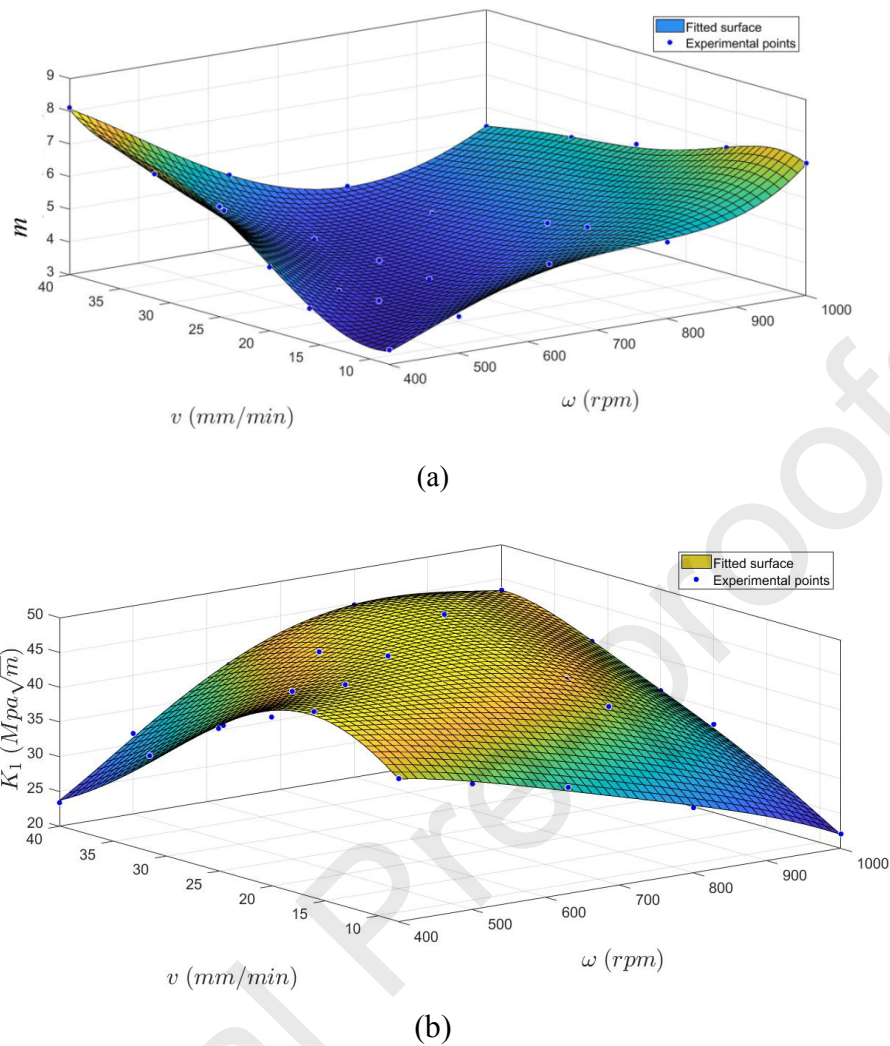
Figure 9. The fitted surface for; a) m, and b) K_I.

4.4. Comparing Artificial neural network and Fitting Results

It can be seen in Figure 10 that the absolute values of errors for *m* and K_I in ANN are smaller than the fitting method. In addition, maximum values of error of ANN and fitting method for *m* are 0.2726 and 0.3225 respectively. Also, the maximum value of the error of ANN and fitting method for K_I are 1.4913 and 1.8263 respectively. Comparing the ANN and fitting methods, it can be understood that the ANN can better predict slope (*m*) and fracture toughness and the correlation coefficient for the fitting method are not calculated. As ANN is more accurate, it is used as the cost function calculator in the optimization algorithm.
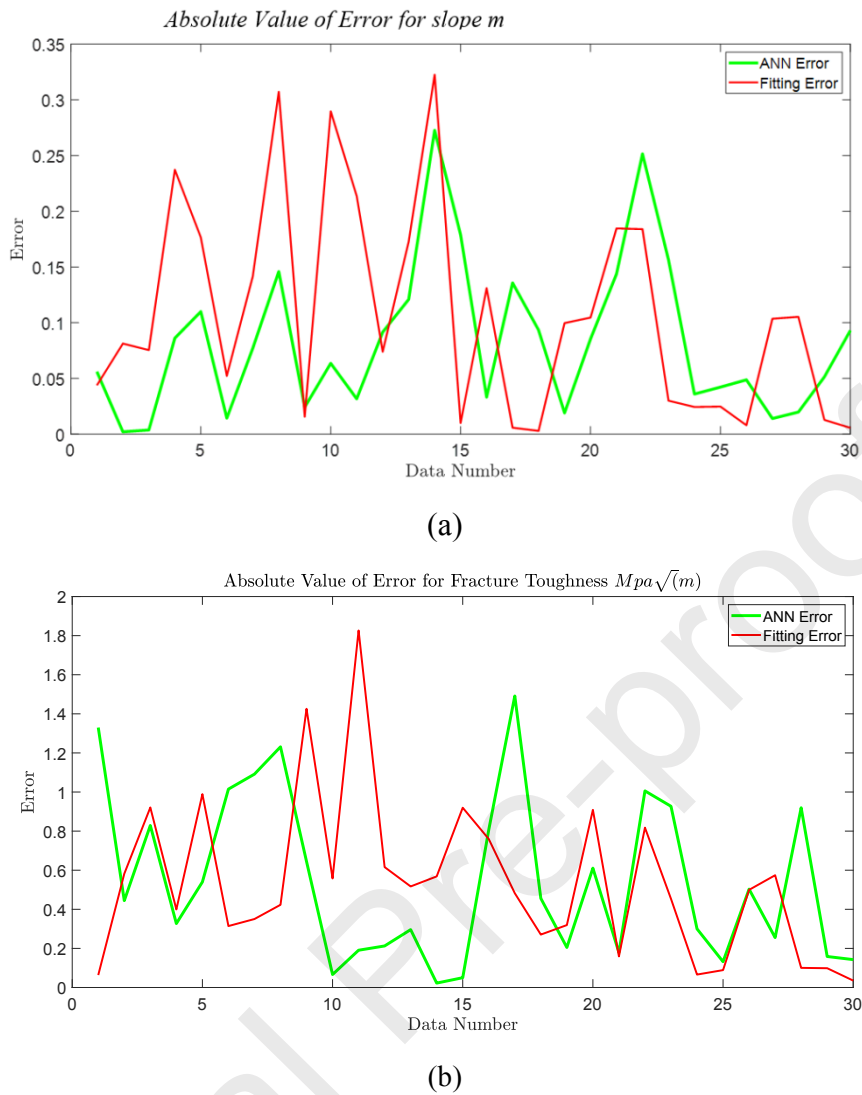
18

(a)

(b)

Figure 10. Absolute value of error for; a) *m,* and b) K_I.

4.5. Multi optimization of welding parameters results

Generally, in multi-objective optimization, a set of results are obtained and as all these results are obtained from the first front (Pareto front) there is not any priority in selecting them. The final Pareto front of optimization is presented in Figure 11. The obtained *m* and K_I versus ω and *v* are shown in Figure 12. Also, the obtained results from Pareto front are presented in Table 9.
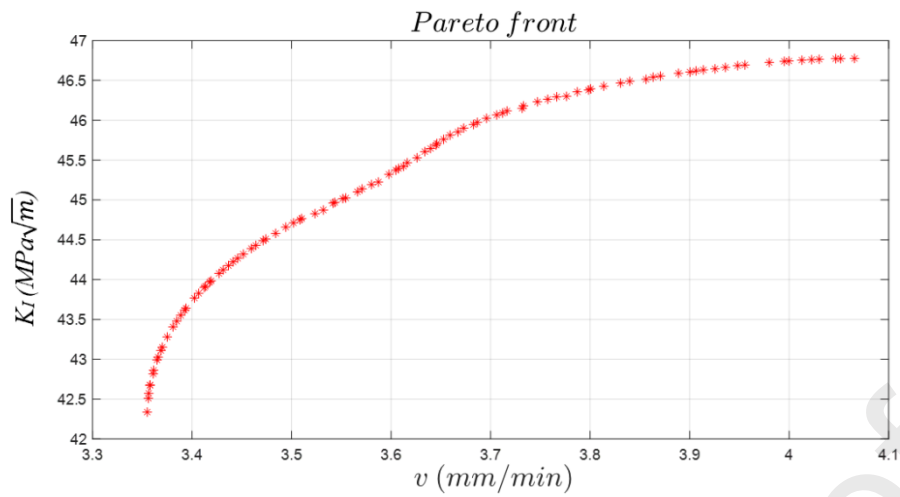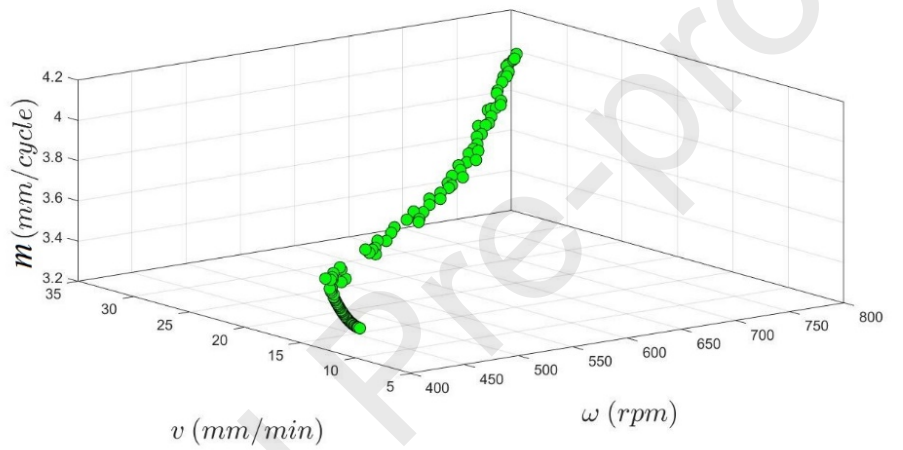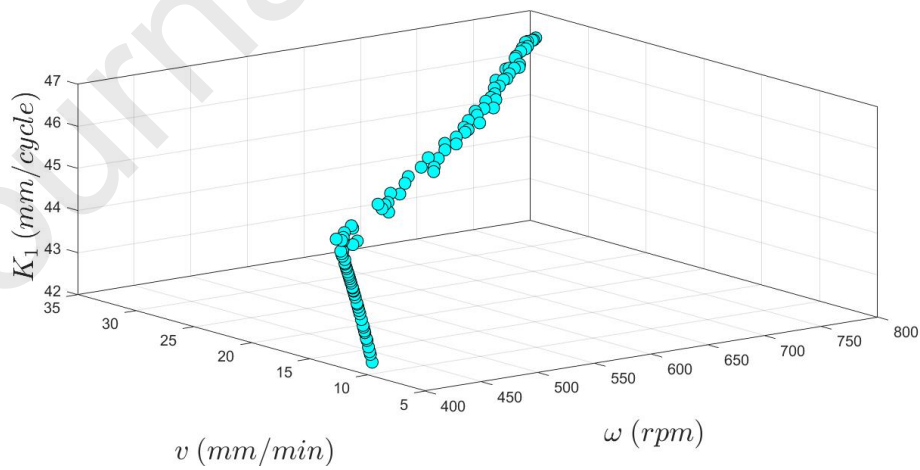
19

Figure 11. The obtained results from the final Pareto front of optimization.

(a)

(b)

Figure 12. The obtained results from the final Pareto front; a) m versus ω and v, and b) K_I

versus ω and v.

20

Table 9. The obtained results from Pareto front.

ω	v	m	K_I	ω	v	m	K_I
766.3934	31.25161	4.06569	46.77531	400.064	10.36197	3.370227	43.15156
400	9.564814	3.355004	42.33726	400.1503	10.02763	3.361012	42.81784
400	10.49425	3.375108	43.28006	673.4258	25.31172	3.839765	46.48978
734.9261	29.48058	3.980039	46.72442	687.1606	25.99759	3.870633	46.55448
401.2284	12.0494	3.484039	44.58019	500.7778	16.58666	3.633879	45.60656
400.0106	11.02487	3.402432	43.76796	681.4423	26.38966	3.856282	46.51341
661.0202	24.48254	3.813745	46.4277	400	10.06927	3.361432	42.86224
461.2495	14.70439	3.597851	45.32081	400	11.09251	3.406697	43.82753
400	10.62782	3.380928	43.4065	400.0154	10.70509	3.38465	43.47834
479.469	15.7417	3.62608	45.52916	400	10.19875	3.36481	42.99198
400.0585	9.728251	3.356143	42.50979	488.2793	15.80817	3.616328	45.46706
420.6937	12.87288	3.531969	44.87329	642.6331	22.80455	3.776279	46.29986
400	12.13455	3.494211	44.65867	565.2621	19.43719	3.672939	45.90093
414.7038	12.67376	3.523613	44.82799	421.0629	13.42132	3.580369	45.19292
725.2179	28.929	3.955578	46.6943	400	11.77579	3.459605	44.39078
466.4249	14.62949	3.587321	45.22428	400.0087	10.78392	3.388649	43.55112
695.244	26.576	3.888888	46.5896	529.2037	17.96095	3.652848	45.75976
624.6872	22.46699	3.747088	46.23115	629.0875	23.05608	3.757461	46.26298
669.0215	25.31172	3.830574	46.46545	602.6645	21.44957	3.716513	46.11634
646.984	23.89747	3.787142	46.35595	551.8326	18.69336	3.659292	45.81244
410.8893	13.03175	3.566248	45.10273	400	12.20906	3.501965	44.71183
400	11.38485	3.427195	44.07685	713.9019	27.51538	3.935954	46.66313
586.8185	20.56047	3.695944	46.0243	421.3355	13.32897	3.570858	45.13794
400	10.88145	3.39394	43.64	400	12.67376	3.554584	45.02381

In all the presented results, the values of m are minimized and the values of K_I are maximized. It can be seen that there is a variety of optimal cases. Therefore, by selecting one of the adjustments for ω or v the slope (m) of FCP rate is decreased and the fracture toughness is increased.
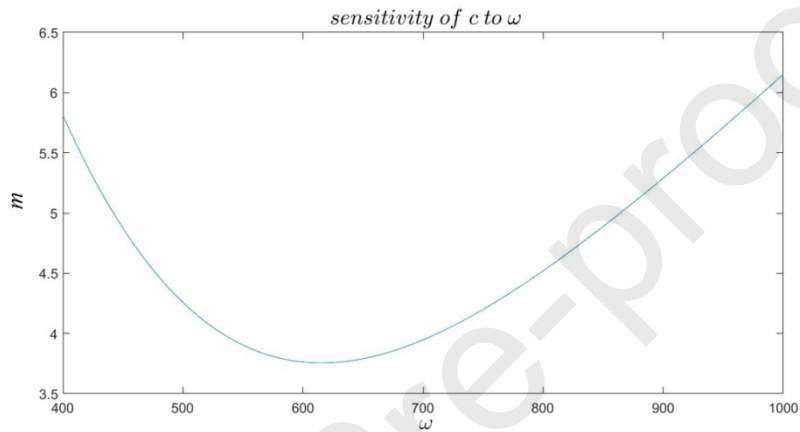
4.6. Sensitivity analysis

To have a better understanding of the behavior of output sensitivity analysis is used. It determines how a dependent variable is affected by different values of an independent variable. In the current work, the slope (m) of FCP rate and fracture toughness are outputs of the model

21

and rotational speed and traverse speed are independent variables. By sensitivity analysis, the relationship and effect of each input parameter on the outputs are evaluated. For instance, for a function based on the independent variables such as Eq. (8).

$$output = f\left(x_1, x_2, x_3, ..., x_n\right) \tag{8}$$

By fixing $n-1$ variables on their average values and changing the remained variable in its range, the output value is calculated. Therefore, the behavior of output based on one parameter can be obtained. In this work, the sensitivity analysis for both slope (m) and fracture toughness are calculated. In Figure 13-a to Figure 13-d, sensitivity analysis is presented.
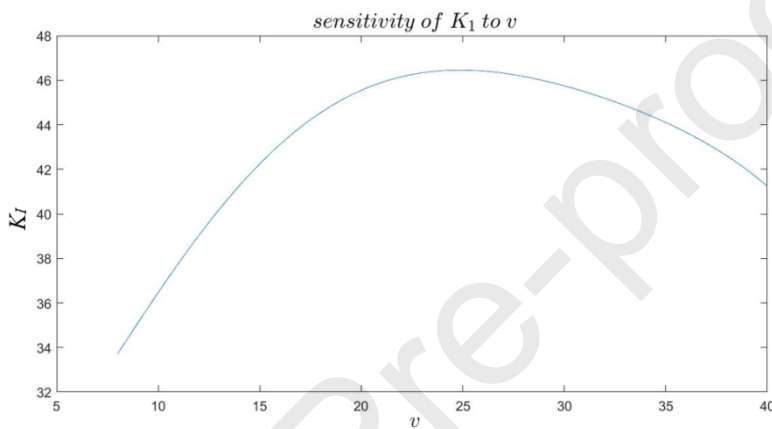
(a)

(b)

22
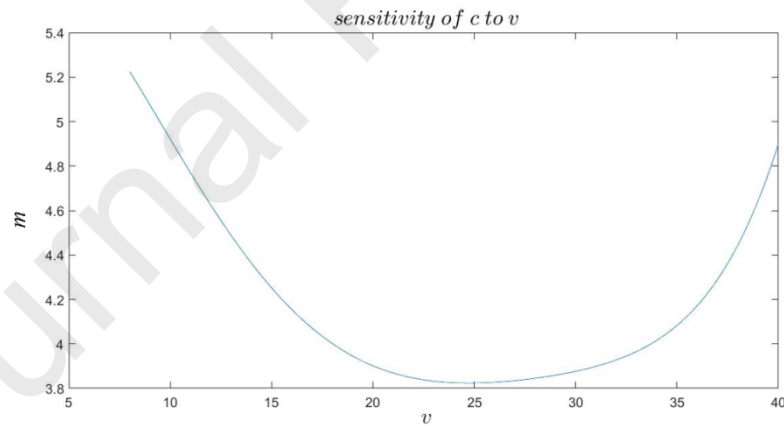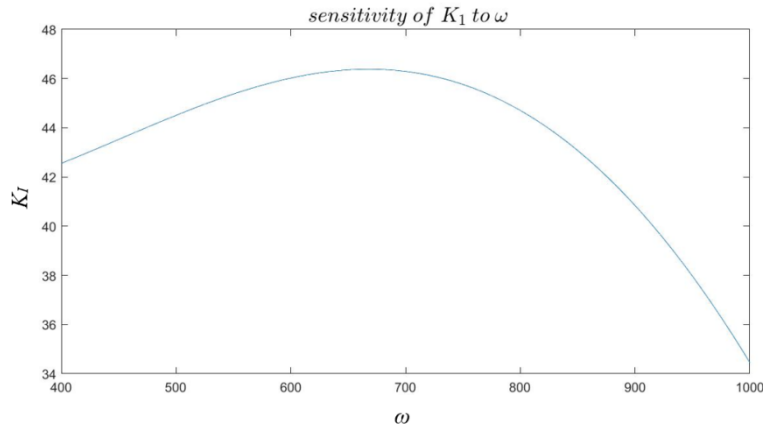
(c)

(d)

Figure 13. The sensitivity analysis for; a) c to ω, b) c to v, c) K_I to ω, and d) K_I to v.

The sensitivity of slope (m) based on the rotational speed is presented in Figure 13-a. It can be seen that in 600 rpm, the value of m is less affected by the rotational speed and in the corners of the interval, its effect on this output is increased. The sensitivity of slope (m) based on the traverse speed is presented in Figure 13-b. It can be seen that in 25 mm/min, the value of m is less affected by the traverse speed and in the corners of this interval, its effect on this output is increased. The sensitivity of fracture toughness based on the rotational speed is presented in Figure 13-c. It can be seen that in 700 rpm, the value of K_I is highly affected by the rotational speed and in 1000 rpm, its effect on this output is minimum. The sensitivity of fracture toughness based on the traverse speed is presented in Figure 13-d. It can be seen that in 25mm/min the value of K_I is highly affected by the rotational speed and in 8 mm/min, its effect on this output is minimum. It can be understood that when ω and v have their mean value, they have the smallest effect on m but have the highest effect on K_I.

23

5. Conclusions

In this paper, an artificial neural network is used to predict the slope of FCP rate (m) and fracture toughness $\left(K_I\right)$. Also using a fitting method, two surfaces are obtained which illustrate the behavior of m, K_I and a mathematical formula for predicting these values based on the ω and v are extracted. These methods can reduce the lab costs by predicting the behavior of stir welding and can eliminating extra lab tests. Both ANN and fitting methods are useful for prediction of welding but by comparing the results, the ANN had better accuracy in predicting K_I and the slope of m compared to the surface fitting method. Also, for the first time, multi-objective optimization is performed to minimize m and maximize K_I. Finally, the sensitivity analysis is applied to obtain the effect of rotational and traverse speeds on the stir welding 2024-T351 aluminum alloy.

References

[1] Masoudi Nejad, Reza, S.M. Salehi, G.H. Farrahi, and M. Chamani. "Simulation of crack propagation of fatigue in Iran rail road wheels and Effect of residual stresses." In: Proceedings of the 21st International Conference on Mechanical Engineering, Iran, 2013.

[2] Reza Masoudi Nejad, Mohammadreza Tohidi, Ahmad Jalayerian Darbandi, Amin Saber, Mahmoud Shariati. "Experimental and numerical investigation of fatigue crack growth behavior and optimizing fatigue life of riveted joints in Al-alloy 2024 plates." Theoretical and Applied Fracture Mechanics, 108, 102669 (2020).

[3] Aliakbari, Karim, Mohammad Imanparast, and Reza Masoudi Nejad. "Microstructure and fatigue fracture mechanism for a heavy-duty truck diesel engine crankshaft." Scientia Iranica, 26(6), pp. 3313-3324 (2019).

[4] Shariati M., Mirzaei M., and Masoudi Nejad R., "An applied method for fatigue life assessment of engineering components using rigid-insert crack closure model", Engineering Fracture Mechanics, 204, pp. 421-433 (2018).

[5] D. Ghahremani Moghadam, and Kh. Farhangdoost. "Influence of welding parameters on fracture toughness and fatigue crack growth rate in friction stir welded nugget of 2024-T351 aluminum alloy joints." Transactions of Nonferrous Metals Society of China 26, no. 10 (2016): 2567-2585.

[6] D. Ghahremani Moghadam, Kh. Farhangdoost, and R. Masoudi Nejad. "Microstructure and residual stress distributions under the influence of welding speed in friction stir welded 2024 aluminum alloy." Metallurgical and Materials Transactions B 47, no. 3 (2016): 2048-2062.

[7] G. D'Urso, C. Giardini, S. Lorenzi, M. Cabrini, and T. Pastore. "The effects of process parameters on mechanical properties and corrosion behavior in friction stir welding of aluminum alloys." Procedia Engineering 183 (2017): 270-276.

[8] S. Rajakumar, and V. Balasubramanian. "Establishing relationships between mechanical properties of aluminium alloys and optimised friction stir welding process parameters." Materials & Design 40 (2012): 17-35.

[9] I. Radisavljevic, A. Zivkovic, N. Radovic, and Vencislav Grabulov. "Influence of FSW parameters on formation quality and mechanical properties of Al 2024-T351 butt welded joints." Transactions of Nonferrous Metals Society of China 23, no. 12 (2013): 3525-3539.

[10] P. Dong, H. Li, D. Sun, W. Gong, and J. Liu, "Effects of welding speed on the microstructure and hardness in friction stir welding joints of 6005A-T6 aluminum alloy," Materials & Design, vol. 45, pp. 524-531, 2013.

[11] J. Kundu, G. Ghangas, N. Rattan, et al. Effect of Different Parameters on Heat Generation and Tensile Strength of FSW AA5083 Joint. International Journal of Current Engineering and Technology. 2017;7(3):1170–1174.

[12] R. Moshwan, F. Yusof, M. Hassan, and S. Rahmat, "Effect of tool rotational speed on force generation, microstructure and mechanical properties of friction stir welded Al–Mg–Cr–Mn (AA 5052) alloy," Materials & Design, vol. 66, pp. 118-128, 2015.

[13] Song W, et al. Fatigue crack growth behavior of Ni-Cr-Mo-V steel welded joints considering strength mismatch effect. Int J Fatigue 2021;151.

[14] Xin H, et al. Probabilistic strain-fatigue life performance based on stochastic analysis of structural and WAAM-stainless steels. Eng Fail Anal 2021;127.

[15] Xin H, et al. Residual stress effects on fatigue life prediction using hardness measurements for butt-welded joints made of high strength steels. Int J Fatigue 2021;147.

[16] Barbosa JF, et al. Fatigue life prediction of metallic materials considering mean stress effects by means of an artificial neural network. Int J Fatigue 2020;135.

[17] Rozumek D, et al. The influence of heat treatment on the behavior of fatigue crack growth in welded joints made of S355 under bending loading. Int J Fatigue 2020;131.

[18] da Silva ALL, et al. Influence of fillet end geometry on fatigue behaviour of welded joints. Int J Fatigue 2019;123:196-212.

[19] W. Macek, R. Branco, M. Korpyś, T. Łagoda, Fractal dimension for bending–torsion fatigue fracture characterisation, Measurement. 184 (2021) 109910.

[20] R. Branco, J.D. Costa, L.P. Borrego, F. Berto, S.M.J. Razavi, W. Macek, Comparison of different one-parameter damage laws and local stress-strain approaches in multiaxial fatigue life assessment of notched components, International Journal of Fatigue. 151 (2021) 106405.

[21] W. Macek, R. Branco, J.D. Costa, C. Pereira, Strain sequence effect on fatigue life and fracture surface topography of 7075-T651 aluminium alloy, Mechanics of Materials. 160 (2021) 103972.

[22] R. Branco, J.D. Costa, J.A. Martins Ferreira, C. Capela, F. v. Antunes, W. Macek, Multiaxial fatigue behaviour of maraging steel produced by selective laser melting, Materials and Design. 201 (2021) 109469.

[23] T. Santos, T. Hermenegildo, C. Afonso, R. Marinho, M. Paes, and A. Ramirez, "Fracture toughness of ISO 3183 X80M (API 5L X80) steel friction stir welds," Engineering Fracture Mechanics, vol. 77, pp. 2937-2945, 2010.

[24] M. K. Kulekci, I. Sevim, and U. Esme, "Fracture toughness of friction stir-welded lap joints of aluminum alloys," Journal of materials engineering and performance, vol. 21, pp. 1260-1265, 2012.

[25] E. Salvati, J. Everaerts, K. Kageyama, and AM. Korsunsky. "Transverse fatigue behaviour and residual stress analyses of double sided FSW aluminium alloy joints." Fatigue & Fracture of Engineering Materials & Structures 42, no. 9 (2019): 1980-1990.

[26] Reza Masoudi Nejad, Zhiliang Liu, Wenchen Ma, Filippo Berto. Fatigue reliability assessment of a pearlitic Grade 900A rail steel subjected to multiple cracks. Engineering Failure Analysis. 2021;128:105625.

[27] Reza Masoudi Nejad, Zhiliang Liu, Wenchen Ma, Filippo Berto. Reliability analysis of fatigue crack growth for rail steel under variable amplitude service loading conditions and wear. International Journal of Fatigue. 2021;152:106450.

[28] Reza Masoudi Nejad. "Numerical study on rolling contact fatigue in rail steel under the influence of periodic overload." Engineering Failure Analysis, 115, 104624 (2020).

[29] Reza Masoudi Nejad. "The effects of periodic overloads on fatigue crack growth in a pearlitic Grade 900A steel used in railway applications." Engineering Failure Analysis, 115, 104687 (2020).

[30] G. D'Urso, C. Giardini, S. Lorenzi, and T. Pastore. "Fatigue crack growth in the welding nugget of FSW joints of a 6060 aluminum alloy." Journal of Materials Processing Technology 214, no. 10 (2014): 2075-2084.

[31] R. Wang, and P. Mi. "Study on fatigue strength of FSW joints of 5083 aluminum alloy with kissing bond defect." Journal of Mechanical Science and Technology 34, no. 7 (2020): 2761-2766.

[32] X. Xu, Q. Liu, S. Qi, H. Hou, J. Wang, and X. Ren. "Effect of incomplete penetration defects on mechanical and fatigue properties of friction-stir-welded 6802-T6 joint." Journal of Materials Research and Technology 15 (2021): 4021-4031.

[33] W.K. Kim, S.T. Won, and B.C. Goo, "A study on mechanical characteristics of the friction stir welded A6005-T5 extrusion," International Journal of Precision Engineering and Manufacturing, vol. 11, pp. 931-936, 2010.

[34] A. Cirello, G. Buffa, L. Fratini, and S. Pasta, "AA6082-T6 friction stir welded joints fatigue resistance: influence of process parameters," Proceedings of the Institution of Mechanical Engineers, Part B: Journal of Engineering Manufacture, vol. 220, pp. 805-811, 2006.

[35] D. Hrishikesh, D. Chakraborty, and T. K. PAL, "High-cycle fatigue behavior of friction stir butt welded 6061 aluminium alloy," Transactions of Nonferrous Metals Society of China, vol. 24, pp. 648-656, 2014.

[36] H. Okuyucu, A. Kurt, and E. Arcaklioglu. "Artificial neural network application to the friction stir welding of aluminum plates." Materials & design 28, no. 1 (2007): 78-84.

[37] A. Ghasemi-Kahrizsangi, SF. Kashani-Bozorg, M. Moshref-Javadi, and M. Sharififar. "Friction stir processing of mild steel/Al 2 O 3 nanocomposite: modeling and experimental studies." Metallography, Microstructure, and Analysis 4, no. 2 (2015): 122-130.

[38] I. Dinaharan, R. Palanivel, N. Murugan, and RF. Laubscher. "Predicting the wear rate of AA6082 aluminum surface composites produced by friction stir processing via artificial neural network." Multidiscipline Modeling in Materials and Structures (2019).

[39] R. Hartl, B. Praehofer, and M. F. Zaeh. "Prediction of the surface quality of friction stir welds by the analysis of process data using Artificial Neural Networks." Proceedings of the Institution of Mechanical Engineers, Part L: Journal of Materials: Design and Applications 234, no. 5 (2020): 732-751.

[40] V. Dehabadi, S. Ghorbanpour, and G. Azimi. "Application of artificial neural network to predict Vickers microhardness of AA6061 friction stir welded sheets." Journal of Central South University 23, no. 9 (2016): 2146-2155.

[41] L.A.C. De Filippis, L.M. Serio, F. Facchini, G. Mummolo, and A.D. Ludovico. "Prediction of the vickers microhardness and ultimate tensile strength of AA5754 H111 friction stir welding butt joints using artificial neural network." Materials 9, no. 11 (2016): 915.

[42] M. Vangalapati, K. Balaji, and A. Gopichand. "ANN modeling and analysis of friction welded AA6061 aluminum alloy." Materials Today: Proceedings 18 (2019): 3357-3364.

[43] R. Vignesh, and R. Padmanaban. "Artificial neural network model for predicting the tensile strength of friction stir welded aluminium alloy AA1100." Materials Today: Proceedings 5, no. 8 (2018): 16716-16723.

[44] R. Palanivel, R. F. Laubscher, I. Dinaharan, and N. Murugan. "Tensile strength prediction of dissimilar friction stir-welded AA6351–AA5083 using artificial neural network technique." Journal of the Brazilian Society of Mechanical Sciences and Engineering 38, no. 6 (2016): 1647-1657.

[45] E. Maleki, "Artificial neural networks application for modeling of friction stir welding effects on mechanical properties of 7075-T6 aluminum alloy." In IOP Conference Series: Materials Science and Engineering, vol. 103, no. 1, p. 012034. IOP Publishing, 2015.

[46] L. Fratini, and G. Buffa. "Continuous dynamic recrystallization phenomena modelling in friction stir welding of aluminium alloys: a neural-network-based approach." Proceedings of the Institution of Mechanical Engineers, Part B: Journal of Engineering Manufacture 221, no. 5 (2007): 857-864.

[47] L. Fratini, and G. Buffa. "Metallurgical phenomena modeling in friction stir welding of aluminium alloys: analytical versus neural network based approaches." Journal of engineering materials and technology 130, no. 3 (2008).

[48] G. Buffa, L. Fratini, and F. Micari. "Mechanical and microstructural properties prediction by artificial neural networks in FSW processes of dual phase titanium alloys." Journal of Manufacturing Processes 14, no. 3 (2012): 289-296.

[49] D. Hebb, The Organization of Behavior. New York: Wiley, (1949). ISBN 978-1-135-63190-1

[50] Haykin (2008) Neural Networks and Learning Machines, 3rd edition.

[51] F. Rosenblatt, (1958). "The Perceptron: A Probabilistic Model For Information Storage And Organization in the Brain". Psychological Review. 65 (6): 386–408.

[52] P.J. Werbos, (1975). Beyond Regression: New Tools for Prediction and Analysis in the Behavioral Sciences.

[53] F. Rosenblatt, (1957). "The Perceptron—a perceiving and recognizing automaton". Report 85-460-1. Cornell Aeronautical Laboratory.

[54] J. Schmidhuber, (2015). "Deep Learning in Neural Networks: An Overview". Neural Networks. 61: 85–117. arXiv:1404.7828. doi:10.1016/j.neunet.2014.09.003. PMID 25462637. S2CID 11715509.

[55] A.G. Ivakhnenko, (1973). Cybernetic Predicting Devices. CCM Information Corporation.

[56] A.G. Ivakhnenko, G. Lapa, (1967). Cybernetics and forecasting techniques. American Elsevier Pub. Co.

[57] P. Werbos, (1982). "Applications of advances in nonlinear sensitivity analysis" (PDF). System modeling and optimization. Springer. pp. 762–770.

[58] A. Standard, "Standard test method for plane-strain fracture toughness of metallic materials," in Part vol. 10, 1984.

[59] A. International, Standard Test Method for Measurement of Fatigue Crack Growth Rates: ASTM International, 2011.

[60] C. Coello, S. Lechuga, M. (2002). "MOPSO: A Proposal for Multiple Objective Particle Swarm Optimization". Congress on Evolutionary Computation (CEC'2002). pp. 1051–1056.

[61] M. Erickson, A. Mayer, and J. Horn. "Multi-objective optimal design of groundwater remediation systems: application of the niched Pareto genetic algorithm (NPGA)." Advances in Water Resources 25, no. 1 (2002): 51-65.

[62] J. Knowles, and D. Corne. "The pareto archived evolution strategy: A new baseline algorithm for pareto multiobjective optimisation." In Proceedings of the 1999 Congress on Evolutionary Computation-CEC99 (Cat. No. 99TH8406), vol. 1, pp. 98-105. IEEE, 1999.

[63] K. Deb, A. Pratap, S. Agarwal, T. Meyarivan, (2002). "A fast and elitist multiobjective genetic algorithm: NSGA-II". IEEE Transactions on Evolutionary Computation. 6 (2): 182.

[64] Y. Yusliza, M.S. Ngadiman, and A.M. Zain. "Overview of NSGA-II for optimizing machining process parameters." Procedia Engineering 15 (2011): 3978-3983.

<u>Highlights</u>

- The FCP rate of the CT specimens of the friction stir welded 2024-T351 aluminum alloys have been studied.

- The effects of rotational and traverse speeds of FSW on the FCP rate and the fracture toughness have been investigated.

- An artificial neural network to predict slope of FCP rate and fracture toughness has been designed.

- Multi-objective optimization algorithm has been used to obtain the best rotational and traverse speeds.

- Sensitivity analysis has been applied to obtain the relationship and effect of rotational and traverse speeds.